THE JOURNAL OF PHYSICAL CHEMISTRY C

Article

Cite This: J. Phys. Chem. C 2018, 122, 29368−29379

pubs.acs.org/JPCC

Exploratory Direct Dynamics Simulations of $^3O_2$ Reaction with Graphene at High Temperatures

Seenivasan Hariharan,[†] Moumita Majumder,[†] Ross Edel,[‡] Tim Grabnic,[‡] S. J. Sibener,[‡] and William L. Hase*,[†]

[†]Department of Chemistry and Biochemistry, Texas Tech University, Lubbock, Texas 79409, United States

[‡]The James Franck Institute and Department of Chemistry, The University of Chicago, 929 East 57th Street, Chicago, Illinois 60637, United States

Supporting Information

ABSTRACT: Direct chemical dynamics simulations at high temperatures of reaction between $^3O_2$ and graphene containing varied number of defects were performed using the VENUS-MOPAC code. Graphene was modeled using (5*a*,6*z*)-periacene, a poly aromatic hydrocarbon with 5 and 6 benzene rings in the armchair and zigzag directions, respectively. Up to six defects were introduced by removing carbon atoms from the basal plane. Usage of the PM7/unrestricted Hartree−Fock (UHF) method, for the simulations, was validated by benchmarking singlet-triplet gaps of *n*-acenes and (5*a*,*nz*) periacenes with high-level theoretical calculations. PM7/UHF calculations showed that graphene with different number of vacancies has different ground electronic states. Dynamics simulations were performed for two $^3O_2$ collision energies E_i of 0.4 and 0.7 eV, with the incident angle normal to the graphene plane at 1375 K. Collisions on graphene with one, two, three, and four vacancies (1C-, 2C-, 3C-, and 4C-vacant graphene) showed no reactive trajectories, mainly due to the nonavailability of reactive sites resulting from nascent site deactivation, a dynamical phenomenon. On the other hand, $^3O_2$ dissociative chemisorption was observed for collisions on four- (with a different morphology), five- and six-vacant graphene (4C-2-, 5C- and 6C-vacant graphene). A strong morphology dependence was observed for the reaction conditions. On all reactive surfaces, larger reaction probabilities were observed for collisions at E_i = 0.7 eV. This is in agreement with the nucleation time measured by supersonic molecular beam experiments wherein about 2.5 times longer nucleation time for O_2 impinging at 0.4 eV compared with 0.7 eV was observed. Reactivity at both collision energies, viz., 0.4 and 0.7 eV, showed the following trend: 5C- < 6C- < 4C-vacant graphene. Formation of carboxyl/semiquinone (C═O)- and ether (−C−O−C−)-type dissociation products was observed on all reactive surfaces, whereas a higher probability of formation of the ether (−C−O−C−) group was found on 4C-vacant graphene on which dangling carbon atoms are present in close proximity. However, no gaseous CO/CO_2 formation was observed on any of the graphene vacancies even for simulations that were run up to 10 ps. This is apparently the result of the absence of excess oxygen atoms that can aid the formation of larger groups, the precursors for CO/CO_2 formation. Although the results of this study do not provide a conclusive understanding of the mechanism of graphene/graphite oxidation, this work serves as an initial study attempting to understand the $^3O_2$ dissociative chemisorption dynamical mechanism on defective-graphene/graphite surfaces at high temperatures.

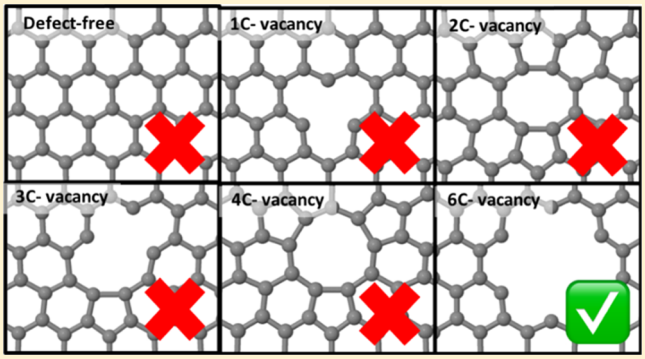

I. INTRODUCTION

Understanding the reaction between molecular oxygen and carbon is of great fundamental and applied interest in the production of fuels from coal,[1] in graphene/graphite oxidation and reduction of graphene oxides,[2] high-temperature gas-cooled nuclear reactors,[3] and degradation of polymeric material in space reentry vehicles.[4] Combustion of carbon by oxygen is generally represented by the following simple equation that has been the backbone of numerous kinetic studies,[5,6]

$$C(s) + \left(1 - \frac{1}{2}x\right)O_2 \rightarrow xCO(g) + (1 - x)CO_2(g)$$

However, considering the number of factors and reactions involved in oxidation of carbon-based surfaces, the reaction mechanism is found to be extremely complex and not very well understood. In particular, details regarding the following remain uncertain, i.e., the nature of adsorbed surface species,

Received: October 17, 2018
Revised: November 25, 2018
Published: November 27, 2018

DOI: 10.1021/acs.jpcc.8b10146
J. Phys. Chem. C 2018, 122, 29368−29379

surface pit depths and shapes, the effects of surface temperature and multiple surface electronic states, and the role of atomistic dynamics for O_2 + C(s) reactions and formation of gaseous products.

Experimental studies using electron microscopy, scanning tunneling microscopy (STM), etc., exhibit formation of etch pits during high-temperature oxidation of highly ordered pyrolytic graphite (HOPG) surfaces.[7−12] However, the ensuing explanation of the oxidation mechanism varied; e.g., active sites on the HOPG basal plane were classified on the basis of the number of free sp^2 orbitals[13] and Monte-Carlo computer models[14] and DFT calculations showed dissociative chemisorption (DC) of O_2 on carbon divacancies.[10] Recently, Delehouzé et al. reported a morphological transition of hexagonal pits at low temperatures to circular pits at high temperatures of ∼1040 K using in situ high-temperature environmental scanning electron microscopy and kinetic Monte-Carlo (kMC) simulations.[15] Interestingly, the transition was observed both at high and low oxygen pressures, which was linked to the competition between etching of armchair and zigzag edge sites of graphene. Recent high-resolution transmission electron microscopy (HRTEM) studies coupled with image simulations[16] showed that oxidation structures contained C═O, pyranlike ether, and lactonelike functional groups. Recent combined experimental and molecular dynamics investigations studied the tendencies of oxidative gasification reaction on carbonized tetracene with zigzag edges and carbonized chrysene with armchair edges[17] and other PAHs.[18] It was found that zigzag edges oxidized and increased their weight whereas armchair edges decomposed without increasing their weight wherein the difference in oxidative gasification was attributed to the difference in activation energy. Similar studies reporting the reactivity of different edges are also available in the literature.[19,20] However, regarding the differences in the etch morphology at different temperatures, no consensus on differences in reactivity of armchair and zigzag edges and subsequent O_2 + C(s) reaction mechanisms has been achieved.

Because of low reactivity of defect-free surfaces,[21−26] interactions of molecular oxygen with carbon vacancies on the basal plane of C(s) surfaces have been investigated theoretically using models for the surface. Using ab initio calculations and a $C_{25}H_9$ model, Chen and Yang found that active site carbons in graphene have a negative charge.[27,28] With theoretical methods and a $C_{25}H_9$ model, Backreedy et al.[29] studying the reactivity of the zigzag edge exposed to O_2 suggested that the defects are active sites with a range of reactivities but sites with dangling carbon atoms are superreactive and subsequently regenerated by a turnover mechanism by a pseudocatalytic mechanism. Using similar models, the following groups have performed detailed quantum chemical calculations to understand O_2 + C(s) reaction mechanism and also differentiate the reactivity of zigzag and armchair type edge sites in graphene. From DFT simulations, Sendt and Haynes[30−33] were able to explain two experimental observations, O_2 adsorption without gasification at low temperatures and O_2 DC followed by desorption at high temperatures. Radovic et al. used quantum chemistry calculations to study various aspects of carbon gasification reactions, including graphene active sites,[34] origin of epoxide groups,[35] thermochemistry of oxygen atom hopping,[36] and nascent site deactivation (NSD),[37] which is responsible for stabilization of reactive/dangling carbon atoms and edge reconstruction. Differences were found for O_2 adsorption on graphene and carbon nanotubes (CNT) and also between the armchair and zigzag edges on both CNT and graphene.[38]

The above studies used an edge-unsaturated model to simulate the reactivity of defect/vacancy sites, which does not completely capture effects of neighboring reactive carbon atoms. In response, O_2 DC was investigated on defective sites of large PAH and supercell models in the following studies. Using the supercell approach, DFT calculations proposed increased chemical reactivity of graphene sheets at relaxed defect structures due to the presence of excess charge assisting dissociation of adsorbed molecules.[39] Later, an ab initio atomistic thermodynamics study[40] proposed a two-step mechanism for low-temperature oxidation of graphene vacancies. It was inferred that increasing the O concentration beyond V4/3O (3 oxygen atoms for 4 vacancies) results in formation of larger oxygen complexes containing anhydride and ether groups. Energetics of adsorption and O_2 DC on various types of defects, such as 1C-vacancy,[41−43] 2C-vacancy,[44,45] and Stone−Thrower−Wales defect,[46] were reported. All of these studies suggested O_2 DC on defect sites, irrespective of the defect number, type, and structure. For dissociative adsorption of OH, H_2O, CO, CO_2, NO, and NO_2, a 1C-vacancy defect showed lower barriers than those of a defect-free graphite surface.[47−49] Although these studies provided valuable insights on the O_2 + graphite reaction mechanism, they missed important dynamical details, such as the fate of dissipated energy and effects of surface temperature, defect morphology, electronic states, etc.

Owing to its relevance in oxidation of polymer-coated surfaces in low-earth orbit, where atomic oxygen species are abundant, collisions of high-energy oxygen atoms with graphite surfaces have been studied in detail using experimental techniques[50−52] and simulations,[53−58] typically at very high energies (∼5 eV). Although understanding the reaction dynamics of atomic oxygen with graphite may assist in explaining the mechanism of carbon gasification/graphite oxidation, it is important to understand differences in reactivity of O and O_2. The O atom is highly reactive and can form epoxide species on a C−C bridge, which is a precursor for further breakup of the hexagonal carbon network. On the contrary, molecular oxygen is first required to dissociate on the "reactive" active sites, followed by migration to the basal plane for carbon removal to occur. Scattering dynamics of hyperthermal O and O_2 on hot vitreous carbon surfaces[59] showed that O was involved in formation of CO_2 at low temperatures and CO and O_2 at high temperatures, wherein no O_2 DC was observed. Similar results were obtained in a photoemission study, supported by DFT calculations probing initial stages of oxidation of perfect and defective HOPG surfaces by atomic oxygen.[60] Furthermore, activation energies calculated over a temperature range of 400−1000 °C showed that at high temperatures, the dissociative chemisorption of O_2 almost entirely dictates the rate of oxidation, with the dissociatively chemisorbed oxygen atoms responsible for desorption of CO and/or CO_2.[61] This clarifies that the reaction mechanisms of O and O_2 with graphite surfaces are fundamentally different.

In a recent review of oxidation of different grades of graphite, different oxidation rates under identical conditions were attributed to differences in surface morphology.[62] To account for this observation, a model based on the intrinsic reaction rate, i.e., the rate normalized to the reactive surface area, was introduced to characterize and understand the role of

DOI: 10.1021/acs.jpcc.8b10146
J. Phys. Chem. C 2018, 122, 29368−29379

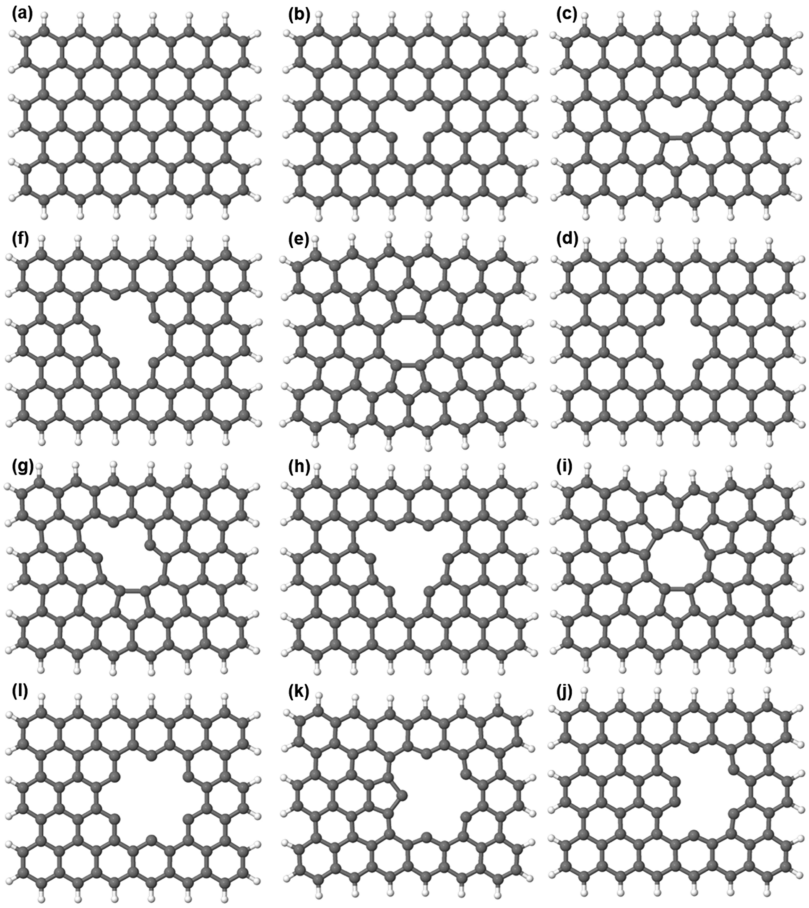

Figure 1. Optimized geometries of (a) defect-free and (b–i) defective-graphene sheets up to six vacancies used as model systems for interaction with $^3O_2$ in direct dynamics simulations. Herein, (b) 1C-vacant unrelaxed, (c) 1C-vacant relaxed, (d) 2C-vacant unrelaxed, (e) 2C-vacant relaxed, (f) 3C-vacant unrelaxed, (g) 3C-vacant relaxed, (h) 4C-1-vacant unrelaxed, (i) 4C-1-vacant relaxed, (j) 4C-2-vacant, (k) 5C-vacant, and (l) 6C-vacant graphene sheets correspond to defective-graphene structures with 1, 1, 2, 2, 3, 3, 4, 4, 4, 5, and 6 carbon atoms removed. Although all structures are optimized, the distinction between unrelaxed and relaxed is explicitly made to show the difference between the two structures only when such distinction could be made. The unconventional way of labeling the figures is chosen to make the comparison between the unrelaxed and relaxed figures easier.

the graphite microstructure and morphology leading to O_2 DC. Since O_2 DC is a difficult step, it is of interest to establish the sufficient and necessary conditions for O_2 dissociation on defective graphene.

Although a substantial number of experimental and theoretical studies have addressed the interaction of O_2 with graphene/graphite surfaces, important questions remain. The starting point of most of the previous studies relied on the assumption that dissociation of O_2 had already been taken place. Furthermore, temperature effects have not been explicitly included, if included, only approximately. As Radovic[34] discussed, "understanding the mechanism of carbon gasification and graphene oxidation is hindered by the lack of knowledge regarding the 'dynamic nature of the reactive surface compounded by the fundamentally different fates of zigzag and armchair sites' ". As discussed above, although the O_2 + C(s) reaction has been widely studied using various experimental and theoretical methods, there have been no dynamics simulations to obtain atomic-level insights into O_2 dissociative chemisorption. A direct dynamics simulation of the oxidation of a single-wall carbon nanotube by singlet O_2 was reported and is a study of the oxidation of a carbon-based material using dynamical methods.[63] However, this study was limited by the number of trajectories and did not consider the reaction of the ground-state triplet O_2.

The current direct dynamics simulation is aimed at obtaining atomistic insights into the dissociative chemisorption of $^3O_2$ on defective-graphene surfaces/sheets at high temperatures. We investigated in detail effects of defect morphology and collision energy on O_2 DC. Since graphite is held together by weak plane–plane van der Waals forces and the mechanism of the interaction of $^3O_2$ with all carbonaceous materials is thought to be similar, in this work, the O_2 + C(s) reaction dynamics were studied using a single graphene layer of carbon atoms. Motivated by studies of the high-temperature oxidation of graphite,[64,65] the reaction was studied at 1375 K. Furthermore, this reaction was studied in the triplet electronic state, the ground electronic state of molecular oxygen. We are aware that other adiabatic states might be the ground states for O_2 reacting with defective graphene with ground states other than singlet. Although studying the ground-state dynamics (for $^3O_2$ on all defective graphene) is a possibility, the low-lying electronic states might require a comparison with the dynamics on other electronic states too. This would be expensive and time consuming considering the size and number of systems studied and will be carried out in future studies. Effect of surface temperature, effects of different electronic states, and

DOI: 10.1021/acs.jpcc.8b10146
J. Phys. Chem. C 2018, 122, 29368–29379

energy-transfer mechanisms will also be the subject of future studies. The manuscript is organized as follows. Details of graphene potential energy surfaces and direct dynamics simulation method are provided in Sections II and III, respectively. Results and discussion are presented in Section IV, and the results are summarized in Section V.

II. GRAPHENE POTENTIAL ENERGY SURFACES

II.I. Ground Electronic State PES of Graphene with Defects. Periacenes, resulting from the peri-condensation of acenes, possessing a balance between the number of zigzag and armchair edges in their periphery, are good models to study graphene. In the current study, graphene is modeled using [5a,6z] periacene (Figure 1a) with 5 and 6 edge benzene rings in the armchair and zigzag directions, respectively. DFT calculations using both atom-centered and plane wave basis set showed that for graphene nanoribbons modeled as periacenes, with at least three consecutive zigzag edges, a spin-polarized state with each edge having an opposite spin is the ground state.[66−69] Further calculations using high-level multireference theories also confirmed the spin-polarized states and the multiradical/polyradical character of periacenes[70] and showed that the singlet−triplet energy gap in model graphene systems approach near-degeneracy for sufficiently extended systems.[71,72] All of these studies emphasized the use of multireference theories when studying graphene.

Although multireference methods might be necessary for the most accurate treatment of graphene, a recent review suggested that semiempirical methods with a dispersion correction may be a good choice to study interaction of molecules with graphene.[73] For the present study PM7,[74] the most recent method incorporated in MOPAC[75] and one that uses a D2-type correction for the H, C, and O atoms considered in this study, is employed. PM7 combined with the unrestricted Hartree−Fock (UHF) Hamiltonian method, best suited for radical systems, is used for all calculations reported here for triplet oxygen interacting with defective-graphene surfaces. UHF was also preferred because the gradient calculation, the critical step in direct dynamics simulations, is much slower with restricted open-shell Hartree−Fock (ROHF). However, with UHF, the wave function is not spin-quantized, a consequence of spin contamination. Nevertheless, PM7/UHF within MOPAC is the best compromise between speed and accuracy.

Prior to using PM7/UHF for the direct dynamics simulations, it was benchmarked with the high-level coupled cluster single and double and perturbative triple excitation (CCSD(T)), multiconfigurational self-consistent field (MCSCF), complete active space self-consistent field (CASSCF), and other multireference (MR) theoretical methods. Comparisons of singlet−triplet energy gaps ($\Delta E_{S\text{-}T}$) calculated for linear *n*-acenes (*n* = 1−7) (Figure S1) and of the (5*a*,*nz*) periacenes (*n* = 2−6) (Figure S2) using PM7/UHF with results obtained from coupled cluster, multireference configuration interaction methods and also from experiment are given in Tables S1 and S2 of the Supporting Information. For linear *n*-acenes, the overall decreasing trend in $\Delta E_{S\text{-}T}$, with increase in *n*, was qualitatively reproduced by PM7/UHF. For linear *n*-acenes, up to *n* = 5, PM7/UHF underestimates $\Delta E_{S\text{-}T}$ whereas agreement with high-level theory methods is better for the linear *n*-acenes with *n* = 6 and 7. Thus, PM7/UHF is a good choice for a system with a large number of rings in the zigzag direction of graphene flakes. Among the (5*a*,*nz*) periacenes with *n* = 2−6, PM7/UHF underestimates $\Delta E_{S\text{-}T}$ for (5*a*,2*z*) periacene whereas it overestimates $\Delta E_{S\text{-}T}$ for (5*a*,*nz*) periacenes with *n* = 3−5. For (5*a*,4*z*) and (5*a*,5*z*) periacenes, the $\Delta E_{S\text{-}T}$ values are high compared with the multireference calculations. Nevertheless, the overall trend showing an initial decrease and then an increase in $\Delta E_{S\text{-}T}$ beyond (5*a*,4*z*) periacenes is qualitatively captured by PM7/UHF.

II.II. Electronic States of Graphene with Vacancies. Previous direct dynamics studies of oxidation of single-wall carbon nanotube noted that the proper choice of electronic state is critical for achieving reliable results in oxygen-carbon reactions.[63] Later, Frankcombe[76] pointed out that it is reasonable to consider that spin states arising from unpaired electrons on the edge carbon atoms are degenerate. In addition, it was also mentioned that the fate of spin states in bond breaking regions is largely unknown. Although the latter statement still holds true, there have been several studies reporting the ground electronic states of graphene flakes/sheets of various sizes and shapes.[70−72,77] Depending upon the level of theory used for the calculations, the ground electronic states of the defect-free graphene varied from a closed shell to open-shell singlet,[68,78] with some systems having near-degenerate singlet and triplet states.

Although the ground electronic states of defect-free graphene systems are well studied, literature on the ground electronic states of defective graphene is scarce.[79−81] When defects are created within graphene, the ground electronic state is different from that for defect-free graphene. Compared with unrelaxed configurations, the ground electronic states are different for relaxed configurations, with structural reconstructions resulting from optimizing positions of reactive/dangling carbon atoms at nascent sites. Given the number of possibilities, it is crucial to determine accurately the ground electronic states for model graphene sheets employed in studies of graphene/graphite oxidation (carbon gasification).

II.III. PM7 Electronic States and PESs. All structures corresponding to defect-free and defective graphene sheets shown in Figure 1 were optimized using PM7/UHF in different electronic states to identify their ground electronic states. Relative energies of different electronic states calculated for defect-free and defective graphene with PM7/UHF are listed in Table 1. Defect-free graphene showed a singlet ground state, with the triplet and quintet states lying 0.80 and 1.08 eV higher in energy, respectively. Unrelaxed 1C-vacant graphene (Figure 1b) with 3 dangling carbon atoms has a quintet ground state, with triplet and singlet states closely lying at 0.12 and 0.18 eV above the ground state. Whereas the relaxed structure with 1 dangling carbon atom had a singlet ground state with relatively low-lying triplet and quintet states compared to those of the defect-free structures. These findings agree well with comparisons of ground and low-lying closed shell singlet excited electronic states of defect-free and monovacant graphene molecules of different sizes. It was found that the first and second excitation energies were significantly lower for monovacant graphene than those calculated for its defect-free counterparts.[81] In addition, it was found that the formation of a vacancy defect in graphene results in the formation of new energy levels.

For 2C-vacant graphene, both unrelaxed and relaxed structures with 4 and 0 dangling carbon atoms (Figure 1d,e), showed quintet ground states with near-degenerate triplet states. The singlet state in both cases lies ∼0.5 eV or higher

DOI: 10.1021/acs.jpcc.8b10146
J. Phys. Chem. C 2018, 122, 29368−29379

Table 1. Structure Optimization and Evolution of Electronic States in Model Graphene Structures Using PM7/UHF[a,bc]

		relative energies, eV		
defects	C*	singlet	triplet	quintet
defect-free	0	**0.00**	0.80	1.08
1C-vacant-UR	3	0.18	0.12	**0.00**
1C-vacant-R	1	**0.00**	0.56	0.77
2C-vacant-UR	4	0.48	0.06	**0.00**
2C-vacant-R	0	0.65	0.02	**0.00**
3C-vacant-UR	5	**0.00**	0.33	0.02
3C-vacant-R	3	**0.00**	0.16	0.06
4C-vacant-1UR	6	0.14	0.49	**0.00**
4C-vacant-1R	0	0.55	**0.00**	0.62
4C-vacant-2	6	0.08	0.86	**0.00**
5C-vacant	5	0.57	0.56	**0.00**
6C-vacant	6	**0.00**	0.51	0.34

[a]UR: unrelaxed, R: relaxed, indices 1 and 2 for R and UR: configuration number in relaxed and unrelaxed structures. [b]C*: number of "reactive"/"dangling" carbon atoms created by removal of carbon atoms from the pristine graphene surface to produce defect sites. [c]The values in bold signifies the ground electronic state for that particular graphene system.

than the ground quintet state. Singlet ground states with near-degenerate quintet states were found for unrelaxed and relaxed 3C-vacant graphene (Figure 1f,g), with triplet states lying 0.33 and 0.16 eV above the ground singlet states, respectively. Both 4C-1-vacant unrelaxed and 4C-2-vacant graphene (Figure 1h,j), with six dangling carbon atoms have a quintet ground state with singlet and triplet states as the next higher electronic states. But the relaxed structure (Figure 1i) with no dangling carbon atoms has a triplet ground state with singlet and quintet excited states lying 0.55 and 0.62 eV higher, respectively. A quintet ground state with near-degenerate singlet and triplet states was found for 5C-vacant graphene (Figure 1k) with 5 dangling carbon atoms. For 6C-vacant graphene (Figure 1l), the electronic states are in the order singlet < quintet < triplet with energies 0.00 < 0.34 < 0.51 eV. Of interest is that no correlation was found between the numbers of dangling carbon atoms and the ground electronic state.

III. DIRECT DYNAMICS SIMULATION METHOD

Direct chemical dynamics simulations were performed using the VENUS chemical dynamics computer program[82,83] coupled with the MOPAC[75] electronic structure computer program. PM7 method[74] with unrestricted Hartree−Fock is used for structure optimization, potential energy surface calculation, and calculating gradients during direct dynamics simulations. Direct dynamics simulations were performed by initiating trajectories with $^3O_2$ + graphene in the triplet electronic state. VENUS includes options for choosing initial conditions for a molecule/surface collision. An initial rotational and vibrational temperature of 10 K was assigned to $^3O_2$, whereas energies for the normal modes of the surface were chosen from the Boltzmann distribution for a surface temperature of 1375 K. For the simulations reported here, zero-point energy is not added to $^3O_2$ or to the surface. The algorithm for selection of initial conditions for a $^3O_2$ + graphene collision have been described previously[84] and are depicted in Figure S3. The initial position and momentum of the incoming $^3O_2$ molecule was chosen with respect to a surface plane and the defect site. The surface plane was defined by atoms NN1, NN2, and NN3. The reaction site is specified by displacing the origin of the surface plane by RX, RY, and RZ from atom NN1 in the reference plane. Herein, RZ = 0 was used. As shown in Figure S3, five coordinates b, θ, ϕ_1, ϕ_2, and s are used to define the position of the center-of-mass and the orientation of $^3O_2$ velocity vector with respect to the surface plane. The two coordinates b and ϕ_1 are used to choose an aiming point on the surface plane. The distance from the defect site b (i.e., the impact parameter) was chosen to vary from 0 to a maximum value of 3.0 Å for graphene sheets up to 4C vacancies, whereas b_{max} = 4.0 Å was used for the 5C- and 6C-vacant graphene sheets, beyond which the dissociation probability approaches zero. The angle ϕ_1 is randomly chosen from a uniform distribution between 0 and 360°. The angle θ between the incoming projectile's velocity vector and the surface normal is chosen to be fixed at θ = 0° with fixed initial collision energies, E_i = 0.4 and 0.7 eV. The angle ϕ_2, for the incoming projectile, is chosen randomly between 0 and 360°. It should be noted that the angle ϕ_2 is redundant in normal collisions and has no impact on the reaction dynamics. $^3O_2$ was randomly oriented with respect to its center of mass and the separation s is chosen as sufficiently large at 12 Å to ensure initially there is no interaction between the gaseous species and the surface.

The trajectories were integrated in time by using the 6th order symplectic integration algorithm[85,86] with a time step of 0.25 fs for all trajectories for a total time of 1 ps within which the dissociative chemisorption was realized in the reactive trajectories. O_2 is considered dissociatively chemisorbed when the distance between the two oxygen atoms becomes larger than 1.5 Å at the end of the trajectory, which was further confirmed by visualizing these trajectories. Functional groups formed on O_2 dissociative chemisorption, and further insights into the reaction mechanism are obtained from these visualizations.

IV. RESULTS AND DISCUSSION

IV.I. Nonreactive Collisions. Direct dynamics simulations of $^3O_2$ collisions with 1C-vacant, 2C-vacant, 3C-vacant, and 4C-vacant-1 graphene sheets, illustrated in Figure 1b,d,f,h with 3, 4, 5, and 6 dangling/reactive carbon atoms, respectively, showed no reactive trajectories. O_2 did not undergo dissociative chemisorption on these defective graphene surfaces, and only direct scattering of O_2 was observed. This observation is in contrast to many theoretical calculations that report dissociative chemisorption of O_2 on 1C-vacant,[41−43] 2C-vacant,[44,45] and 4C-vacant graphene.[40] However, earlier reports mentioned that encounter of the colliding O_2 with the reactive carbon atoms is inhibited due to nascent site deactivation[34] and formation of pentagons[39] surrounding vacancies on graphene nanoflakes/sheets. Although graphene edge structures with pentagons surrounding the vacancies are the preferred low-energy structures, at high temperatures, contribution of structures with carbon dangling bonds toward O_2 dissociative chemisorption cannot be ruled out, provided the reactive sites are not deactivated.

Snapshots of representative trajectories for nonreactive O_2 collisions for each of the graphene sheets are given in the Supporting Information (Figures S4−S7), and the corresponding movies are presented in the Supporting Information (SI_movie1−SI_movie4). For 1C-vacant, 2C-vacant, 3C-vacant, and 4C-vacant structures (Figure 1b,d,f,h), dynamical aspects of reactive edge reconstruction by the formation of

DOI: 10.1021/acs.jpcc.8b10146
J. Phys. Chem. C 2018, 122, 29368−29379

Table 2. Dissociation Probabilities for Oxygen on Graphene Sheets with 4, 5, and 6 Vacancies Corresponding to Structures in Figure 1j–l

		no. of trajectories		no. of reactive trajectories		probability	
no. of vacancies	no. of dangling carbon atoms	0.4 eV	0.7 eV	0.4 eV	0.7 eV	0.4 eV	0.7 eV
4	6	350	350	31	43	0.088	0.123
5	5	450	450	13	27	0.028	0.060
6	6	450	450	35	36	0.077	0.080

pentagons, leading to nascent site deactivation (NSD) prior to O_2 collision, is explicitly shown. From molecular orbital molecular dynamics (MO-MD), such reconstructions were found to occur at temperatures as low as 300 K for 1C-vacant graphene.[87] Using DFT calculations, it was found that armchair sites, which occur in pairs, are deactivated by formation of a triple bond, whereas the fate of adjacent zigzag sites in graphene was found to be more complex.[37]

Similarly, in experiments, a decrease in O_2/O reactivity on carbonaceous surfaces with increasing surface temperature was observed.[88] This decrease was attributed to hysteresis involving removal of active sites at high temperatures and regeneration of active sites at low temperatures.[89] However, we suspect that the decrease in reactivity may be due to NSD, which deactivates surface-active sites at higher temperatures.

IV.II. Reactive Collisions. Collisions of O_2 with 4C-vacant-2, 5C-vacant, and 6C-vacant graphene sheets, corresponding to structures in Figure 1j–l with 6, 5, and 6 dangling/reactive carbon atoms, respectively, showed two types of trajectories, i.e., direct scattering (DS) and dissociative chemisorption (DC). Direct scattering occurs when the reactive/dangling carbon atoms are not accessible to the colliding O_2 molecule, whereas O_2 dissociative chemisorption takes place when the colliding O_2 molecule interacts with the reactive/dangling carbon atom present in the vacancy. Within the simulation time, oxygen atoms for the dissociatively chemisorbed trajectories did not form CO or CO_2 species but remained in the chemisorbed state on the surface-active sites.

Dissociation probabilities of O_2 on graphene sheets with varying number and types of defects are given in Table 2 for incident energies, E_i, of 0.4 and 0.7 eV. On 4C-vacant-2 and 5C-vacant graphene sheets, the respective dissociation probabilities for E_i = 0.7 eV are 1.4 and 2.14 times larger than those for O_2 E_i = 0.4 eV. However, on 6C-vacant graphene, the dissociation probabilities for E_i = 0.4 and 0.7 eV are similar, 7.7×10^{-2} and 8.0×10^{-2}, respectively. These results are in agreement with supersonic molecular beam experiments where the etching of small sputtering-induced vacancies was monitored over time using scanning tunneling microscopy (STM).[64] The instrument used for these experiments has been described previously.[64,90] The relative dissociation probabilities under different experimental conditions were inferred by measuring the nucleation time and the amount of O_2 exposure necessary for product formation to begin and etching to occur. Figure 2 shows the amount of carbon consumed by etching with molecular oxygen impinging at a normal angle on a 1375 K surface at both 0.4 and 0.7 eV kinetic energies. The nucleation time, graphically defined as the x intercept of the linear trends, is about 2.5 times longer for 0.4 eV oxygen, in line with the difference in dissociation probabilities predicted in this paper. Further, the nucleation time does not appear to be strongly related to the subsequent etching rate. The nucleation time for 0.7 eV O_2 remained comparatively short even when its etching rate was lowered

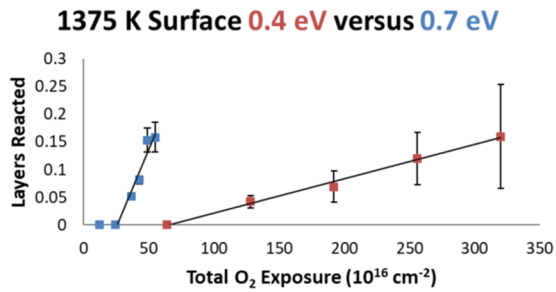

Figure 2. Reactivity of HOPG samples in terms of layers of graphite reacted versus fluence of O_2 from a supersonic molecular beam. Vacancies were introduced by sputtering with 4 keV Ar^+ ions to provide nucleation sites. Samples exposed to molecular oxygen with kinetic energies of 0.4 eV (red) and 0.7 eV (blue) at a surface temperature of 1375 K and normal incident angle show marked differences in nucleation time (the x intercept of the linear regressions) as well as subsequent overall reactivity (the slope). The nucleation time with 0.4 eV oxygen is roughly 2.5 times longer than with 0.7 eV oxygen.

through the use of a higher quality HOPG sample. HOPG samples were supplied by SPI, with the higher quality grade 2 samples having a lower density of domain boundaries and intrinsic defects than that of the lower quality grade 3 samples otherwise used in these experiments. Conversely, altering the impingement angle of the beam affected nucleation time but not the etching rate, with more glancing angles producing longer nucleation times. Thus, the dissociation process is related in some way to the normal component of the O_2 kinetic energy. Taken together, the experimental evidence shows that molecular oxygen with higher energy and impingement angles closer to normal do indeed dissociate more readily on sputter vacancies, leading to a higher coverage of adsorbed O and the onset of product formation at smaller O_2 exposures.

Snapshots of representative trajectories forming two semiquinone (carbonyl, C═O) groups on 4C-vacant-2, 5C-vacant, and 6C-vacant graphene sheets are shown in Figure 3a–c. The corresponding movies are also available in the Supporting Information movies SI_movie5, SI_movie6, and SI_movie7. All above observations are in agreement with Ranish and Walker's study that stated that if the collision event between the nascent sites and oxygen occurs prior to rehybridization, the probability of chemical interaction is markedly enhanced.[91] Our results also agree with the study by Malola et al.,[92] which noted that edge reconstruction chemically passivates the zigzag edge, which also emphasized that spin multiplicities of a free zigzag site are the key issue because both the path and the energetics of its chemical passivation are very much dependent on its geometry.

Direct scattering, a predominant event in these simulations, may occur in both thermal and structural regimes.[93] Direct scattering occurs in the thermal regime when the timescale for

DOI: 10.1021/acs.jpcc.8b10146
J. Phys. Chem. C 2018, 122, 29368–29379

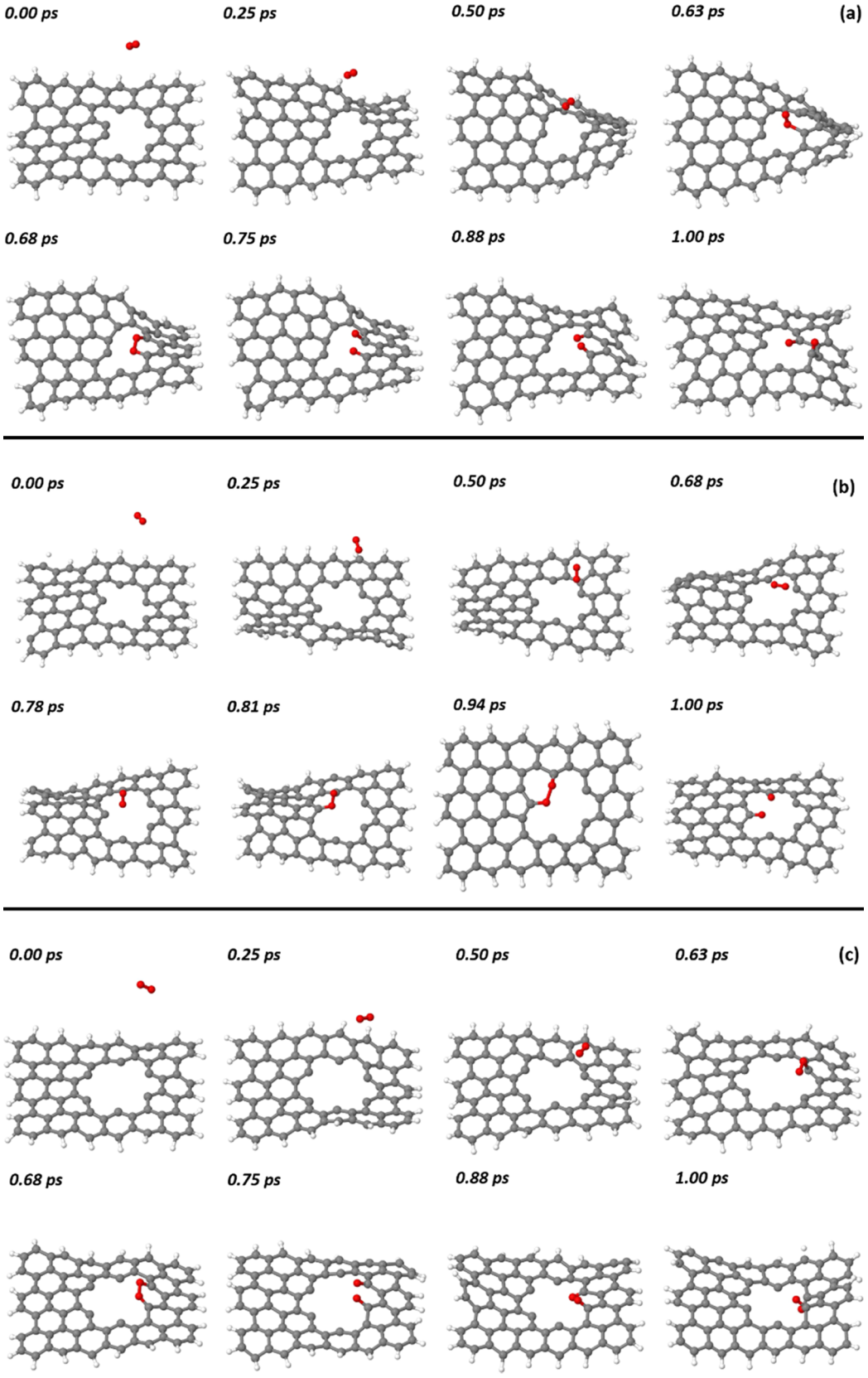

Figure 3. Snapshots from the reactive trajectories of O_2 dissociative chemisorption on (a) 4C-2-, (b) 5C-, and (c) 6C-vacant graphene sheets trajectories in which two semiquinone (-C═O) groups were formed.

E_i is nearly resonant with that for the surface motion with energy $2RT_s$. On the contrary, when E_i is considerably larger, an individual surface atom becomes responsible for repelling the incoming molecule, resulting in collision in the structural regime. At 1375 K, with $2RT_s$ = 0.24 eV, which is smaller than both the incidence energies of 0.4 and 0.7 eV, direct scattering

DOI: 10.1021/acs.jpcc.8b10146
J. Phys. Chem. C 2018, 122, 29368−29379

Table 3. Functional Groups Formed during the Dissociative Chemisorption of O_2 on Graphene Sheets with 4, 5, and 6 Vacancies Corresponding to Structures in Figure 1j–l

		functional groups formed during O_2 dissociative chemisorption					
		0.4 eV			0.7 eV		
no. of vacancies	no. of reactive carbon atoms	2C═O	2−C−O−C−	1C═O and 1−C−O−C−	2C═O	2−C−O−C−	1C═O and 1−C−O−C−
4	6	17	5	9	16	4	23
5	5	10	1	2	23	0	4
6	6	30	0	5	31	0	5

clearly occurs in the structural regime. This observation supports the structure/morphology dependence of O_2 dissociative chemisorption found in this study.

IV.III. Formation of Functional Groups. Depending upon the orientation of the colliding O_2, dissociative chemisorption can occur on reactive sites either adjacent or opposite to the site at which O_2 is chemisorbed. Ether (−C−O−C−) group formation always occurs after formation of the semiquinone (C═O) group, if and only if reactive sites are in close proximity. However, a nearby reactive site does not always guarantee the formation of an ether group. On 5C-vacant graphene, dissociation is always delayed compared with both 4C-vacant-2- and 6C-vacant graphene sheets, because O_2 which approaches the two adjacent reactive sites is repelled by those sites or attracted by the single reactive site present on the pentagon on the opposite side, on which dissociative chemisorption occurs. Depending on the proximity and availability of neighboring sites, CO formation and subsequent ether group formation may occur. These findings agree with the proposition of Radovic,[34] which states that dissociation of O_2 on the zigzag edge is possible. However, it requires the existence of two adjacent free, reactive sites but is an improbable event.

Chemisorbed O_2 reaches out to the nearest carbon atom to dissociatively chemisorb as two semiquinone (C═O), one C═O, and either one ether (−C−O−C−) or two ether groups. Irrespective of the final structure, dissociative chemisorption always occurs through a cyclic intermediate. Availability of an additional reactive C atom for formation of the cyclic intermediate strongly depends on the direction of the vibrational motion of the surface carbon atom and the orientation of the incoming O_2. Previous reports showed that, for two O adatoms, the lowest-energy structure consists of a pair of neighboring ether and carbonyl groups, which is 0.37 eV lower than that of the structure containing two epoxy groups.[55] However, for the current study, the presence of two O adsorbates did not result in formation of epoxy groups but did result in carbonyl, ether, and lactone groups (Table 3). Although previous studies show that bare vacancies are quickly saturated by ether and carbonyl groups, only the formation of larger groups, such as lactones, anhydrides, and carbonate groups, facilitates desorption of CO/CO_2, whose formation requires subsequent collisions of more than one O_2.[40] In addition, within the time of the simulation, regeneration of molecular oxygen was not found in any of these trajectories.

A few reactive trajectories for O_2 + 6C-vacant graphene were run up to 10 ps to check for possible carbon removal by CO/CO_2 formation. In these simulations, no carbon removal via CO/CO_2 formation was observed. Carbon removal did occur through an intermediate step with O migration/spillover from reactive sites, with a complex mechanism.[35] It was previously found that energy cannot be readily dissipated via migration reactions when the graphene domain size is small.[33] Since migration reactions (and subsequent desorption) are less probable on smaller graphene, these surfaces tend to retain oxides at much higher temperatures and probably for longer times compared with highly ordered graphite surfaces. Studies regarding these dynamics might provide valuable information on the timescale for carbon removal via CO/CO_2 formation.

IV.IV. Coalescence of Defects. High-energy Ar^+-ion collision is one of the widely used experimental techniques to produce vacancies on graphene/graphite surfaces to make it reactive. Previous investigations on Ar^+-ion impact on graphene/graphite surfaces reported formation of predominantly 1C-vacant and 2C-vacant defects.[94] However, in our simulations at high temperature (1375 K), 1C-vacant, 2C-vacant, 3C-vacant, and 4C-vacant sites are found to be nonreactive toward O_2. This leaves an interesting question: what defect type and structure is necessary and sufficient to initiate the carbon-oxygen reaction? In experiments, such high temperatures are achieved by heating the sputtered sample to a desired temperature using a direct current heater for the duration of the exposure.[64] At these high temperatures, surface carbon atoms undergo vibrational motion in parallel and perpendicular directions. As mentioned above, Ar^+-ion irradiation in experiments produces multiple monolayer vacancies on the HOPG surface. On annealing, to achieve the desired temperature, the presence of more than one defect resulting from the high dosing of Ar^+ ions may result in structural relaxations of the vacancy-type defects to coalesce into larger defects.[95,96] This observation supports our results in which O_2 DC is only observed for defects larger than 4C-vacant graphene and not on 1C-vacant, 2C-vacant, and 3C-vacant graphene systems. This is contrary to the popular view that 1C-vacant and 2C-vacant sites may be the reaction initiation centers on graphite surfaces. Although predominantly 1C-vacant and 2C-vacant sites are produced during initial Ar^+-ion irradiation, at high temperatures at which O_2 dosing takes place, these defects may coalesce to form larger defects that act as reaction centers.

In most of the early DFT calculations,[31,32,34,38,42,45] the number of configurations considered to explain graphene oxidation is quite small compared with the ones realized in typical direct dynamics simulations. In addition, most calculations do not consider the singlet−triplet transition during adsorption and dissociation and more importantly, do not account for surface temperature effects and the fate of the energy released during the exothermic O_2 dissociative chemisorption reaction. Furthermore, the number of orientations considered for O_2 is also not sufficient to adequately sample the reaction phase space. Experiments indicate that CO and CO_2 formation are facilitated through the formation of larger groups like lactones or a ether−lactone combination, which necessitates the presence of more than two oxygens atoms on the surface. Even after this study, a number of questions remain open. Nevertheless, this study is a first step

DOI: 10.1021/acs.jpcc.8b10146
J. Phys. Chem. C 2018, 122, 29368−29379

toward understanding the reaction dynamics of molecular oxygen with graphene/graphite, although to realize carbon removal in the form of CO/CO_2, further O_2 dosing would be necessary.

V. CONCLUSIONS

Direct dynamics simulations were performed to study the reaction of $^3O_2$ on defective graphene at high temperatures. Dissociative chemisorption of $^3O_2$ was not observed on graphene with 1-, 2-, 3-, and 4-carbon vacancies for the reaction conditions employed in this study. DC of O_2 occurred only on exposed dangling carbon atoms at the defects via a cyclic intermediate and strongly depends on the defect morphology. The necessary condition for oxygen DC at defects is that the carbon atoms at the periphery of the defects should not be close enough to form a C−C bond during the dynamics, resulting in nascent site deactivation (NSD). However, the availability of the nearby reactive site is dynamic and depends on the surface temperature. The dangling/reactive carbon atoms should be exposed during the collision for O_2 to dissociate. Dissociation of molecular oxygen resulted in formation of predominantly carbonyl/semiquinone (C═O) and ether (−C−O−C−) groups. The probability of both adsorbed functional groups being carbonyl or ether depends on the defect morphology. This study strongly establishes that the graphite oxidation mechanisms by atomic oxygen and molecular oxygen are characteristically different.

No CO/CO_2 formation was observed in the (few) simulations run up to 10 ps (at 1375 K and E_i = 0.4 eV). Furthermore, since CO and CO_2 formation are facilitated through the formation of larger groups like lactones or an ether−lactone combination, presence of more than two oxygens atoms on the surface is necessary for carbon removal to take place. Our future studies are directed toward direct dynamics simulations of subsequent collisions of O_2 on a surface containing adsorbed O atoms in multiples of two and collision of O_2 on oxygen preadsorbed at random positions on graphene sheets. In addition, the effect of the adsorption sites, adsorption configuration, and the proximity of adsorbed O atoms to the defects will also be studied to obtain detailed insights into the mechanism of CO/CO_2 removal. Carbon removal and the pit growth on graphene and graphite are expected to be different due to the layered structure of graphite wherein O interactions with the inner graphite layers may lead to a different mechanism compared to that observed on graphene surfaces. Above all, oxygen having a triplet ground state and with graphene exhibiting different electronic ground states for different numbers of vacancies, nonadiabatic dynamics may be necessary to correctly describe crossings between electronic states that may occur within the interaction region, just prior to dissociative chemisorption.

■ ASSOCIATED CONTENT

Supporting Information

The Supporting Information is available free of charge on the ACS Publications website at DOI: 10.1021/acs.jpcc.8b10146.

Structures of linear *n*-acenes (Figure S1) and (5*a*,*nz*) periacenes (Figure S2) used for calculating singlet−triplet energy gaps (Tables S1 and S2) using PM7/UHF Hamiltonian; definition of coordinates used for sampling the trajectory initial conditions (Figure S3); snapshots of representative nonreactive trajectory and nascent site deactivation: O_2 + 1C-vacant (Figure S4), O_2 + 2C-vacant (Figure S5), O_2 + 3C-vacant (Figure S6), and O_2 + 4C-vacant (Figure S7) graphene; snapshots of trajectories with one or two ether groups (−C−O−C−) on O_2 + 4C-vacant-2 graphene (Figure S8); snapshots of trajectories with one semiquinone and one ether (−C−O−C−): O_2 + 4C-vacant-2 (Figure S9), O_2 + 5C-vacant (Figure S10), and O_2 + 6C-vacant (Figure S11) graphene (PDF)

Representative trajectory for nonreactive O_2 collision on 1C-vacant graphene (AVI)

Representative trajectory for nonreactive O_2 collision on 2C-vacant graphene (AVI)

Representative trajectory for nonreactive O_2 collision on 3C-vacant graphene (AVI)

Representative trajectory for nonreactive O_2 collision on 4C-vacant-1 graphene (AVI)

Representative trajectory for O_2 reactive collision leading to the formation of two semiquinone groups on 4C-vacant-2 graphene (AVI)

Representative trajectory for O_2 reactive collision leading to the formation of two semiquinone groups on 5C-vacant graphene (AVI)

Representative trajectory for O_2 reactive collision leading to the formation of two semiquinone groups on 6C-vacant graphene (AVI)

■ AUTHOR INFORMATION

Corresponding Author

*E-mail: bill.hase@ttu.edu.

ORCID

Seenivasan Hariharan: 0000-0003-4509-8454

Moumita Majumder: 0000-0003-3928-957X

S. J. Sibener: 0000-0002-5298-5484

William L. Hase: 0000-0002-0560-5100

Notes

The authors declare no competing financial interest.

■ ACKNOWLEDGMENTS

The research reported here is based upon work supported by the Air Force Office of Scientific Research (AFOSR) Grant FA9550-16-1-0133 and the Robert A. Welch Foundation Grant D-0005. Theoretical calculations were performed on the high-performance computer clusters, Hrothgar and Quanah, maintained by High Performance Computing Center (HPCC) at Texas Tech University, under the direction of Alan Sill. Some parts of the computational calculations were also performed on the Chemdynm cluster of the Hase Research Group. S.J.S. acknowledges support by the Air Force Office of Scientific Research, Grant No. FA9550-15-1-0428, with focus on graphite erosion and ablation, and the NSF, Grant No. CHE-1566364, with focus on spatiotemporal reaction kinetics. Support from the NSF-Materials Research Science and Engineering Center at the University of Chicago, Grant No. NSF-DMR-14-20709, is also gratefully acknowledged.

■ REFERENCES

(1) Breault, R. W. Gasification Processes Old and New: A Basic Review of the Major Technologies. *Energies* **2010**, *3*, 216−240.

(2) Gao, X.; Zhao, Y.; Chen, Z. From Graphene to Graphene Oxide and Back. *Graphene Chemistry: Theoretical Perspectives*; Jiang, D.-E., Chen, Z., Eds.; John Wiley & Sons, Ltd: Chichester, UK, 2013.

(3) Kane, J. J.; Contescu, C. I.; Smith, R. E.; Strydom, G.; Windes, W. E. Understanding the Reaction of Nuclear Graphite with Molecular Oxygen: Kinetics, Transport, and Structural Evolution. *J. Nucl. Mater.* **2017**, *493*, 343−367.
(4) Reddy, M. R. Effect of Low Earth Orbit Atomic Oxygen on Spacecraft Materials. *J. Mater. Sci.* **1995**, *30*, 281−307.
(5) Backreedy, R.; Jones, J. M.; Pourkashanian, M.; Williams, A. A Study of the Reaction of Oxygen with Graphite: Model Chemistry. *Faraday Discuss.* **2001**, *119*, 385−394.
(6) Haynes, B. S. A Turnover Model for Carbon Reactivity I. Development. *Combust. Flame* **2001**, *126*, 1421−1432.
(7) Yang, R. T.; Wong, C. Mechanism of Single-Layer Graphite Oxidation: Evaluation by Electron Microscopy. *Science* **1981**, *214*, 437.
(8) Chang, H.; Bard, A. J. Formation of Monolayer Pits of Controlled Nanometer Size on Highly Oriented Pyrolytic Graphite by Gasification Reactions as Studied by Scanning Tunneling Microscopy. *J. Am. Chem. Soc.* **1990**, *112*, 4598−4599.
(9) Stevens, F.; Kolodny, L. A.; Beebe, T. P., Jr. Kinetics of Graphite Oxidation: Monolayer and Multilayer Etch Pits in HOPG Studied by STM. *J. Phys. Chem. B* **1998**, *102*, 10799−10804.
(10) Hahn, J. R.; Kang, H.; Lee, S. M.; Lee, Y. H. Mechanistic Study of Defect-Induced Oxidation of Graphite. *J. Phys. Chem. B* **1999**, *103*, 9944−9951.
(11) Hahn, J. R. Kinetic Study of Graphite Oxidation Along Two Lattice Directions. *Carbon* **2005**, *43*, 1506−1511.
(12) Theodosiou, A.; Jones, A. N.; Marsden, B. J. Thermal Oxidation of Nuclear Graphite: A Large Scale Waste Treatment Option. *PLoS One* **2017**, *12*, No. e0182860.
(13) Chang, H.; Bard, A. J. Scanning Tunneling Microscopy Studies of Carbon-Oxygen Reactions on Highly Oriented Pyrolytic Graphite. *J. Am. Chem. Soc.* **1991**, *113*, 5588−5596.
(14) Stevens, F.; Beebe, T. P., Jr. Computer Modeling of Graphite Oxidation: Differences Between Monolayer and Multilayer Etching. *Comput. Chem.* **1999**, *23*, 175−183.
(15) Delehouzé, A.; Rebillat, F.; Weisbecker, P.; Leyssale, J.-M.; Epherre, J.-F.; Labrugére, C.; Vignoles, G. L. Temperature Induced Transition from Hexagonal to Circular Pits in Graphite Oxidation by O_2. *Appl. Phys. Lett.* **2011**, *99*, No. 044102.
(16) Yamada, Y.; Murota, K.; Fujita, R.; Kim, J.; Watanabe, A.; Nakamura, M.; Sato, S.; Hata, K.; Ercius, P.; Ciston, J.; et al. Subnanometer Vacancy Defects Introduced on Graphene by Oxygen Gas. *J. Am. Chem. Soc.* **2014**, *136*, 2232−2235.
(17) Yamada, Y.; Kawai, M.; Yorimitsu, Y.; Otsuka, S.; Takanashi, M.; Sato, S. Carbon Materials with Zigzag and Armchair Edges. *ACS Appl. Mater. Interfaces 10* 40710 40739. DOI: 10.1021/acsami.8b11022.
(18) Senda, T.; Yamada, Y.; Morimoto, M.; Nono, N.; Sogabe, T.; Kubo, S.; Sato, S. Analyses of Oxidation Process for Isotropic Pitch-Based Carbon Fiber using Model Compounds. *Carbon* **2019**, *142*, 311−326.
(19) Xu, K.; Ye, P. D. Theoretical Study on the Oxidation Mechanism and Dynamics of the Zigzag Graphene Nanoribbon Edge by Oxygen and Ozone. *J. Phys. Chem. C* **2014**, *118*, 10400−10407.
(20) Chaparala, S. V.; Raj, A. Reaction Mechanism for the Oxidation of Zigzag Site on Polycyclic Aromatic Hydrocarbons in Soot by O_2. *Combust. Flame* **2016**, *165*, 21−33.
(21) Sorescu, D. C.; Jordan, K. D.; Avouris, P. Theoretical Study of Oxygen Adsorption on Graphite and the (8, 0) Single-Walled Carbon Nanotube. *J. Phys. Chem. B* **2001**, *105*, 11227−11232.
(22) Giannozzi, P.; Car, R.; Scoles, G. Oxygen Adsorption on Graphite and Nanotubes. *J. Chem. Phys.* **2003**, *118*, 1003−1006.
(23) Ricca, A.; Drocco, J. A. Interaction of O_2 with a (9, 0) Carbon Nanotube. *Chem. Phys. Lett.* **2002**, *362*, 217−223.
(24) Lamoen, D.; Persson, B. N. J. Adsorption of Potassium and Oxygen on Graphite: A Theoretical Study. *J. Chem. Phys.* **1998**, *108*, 3332−3341.
(25) Morón, V.; Gamallo, P.; Sayós, R. DFT and Kinetic Study of O/O_2 Mixtures Reacting over a Graphite (0001) Basal Surface. *Theor. Chem. Acc.* **2011**, *128*, 683−694.
(26) Yan, H. J.; XU, B.; Shi, S. Q.; Ouyang, C. Y. J. First−Principles Study of the Oxygen Adsorption and Dissociation on Graphene and Nitrogen Doped Graphene for Li-Air Batteries. *J. Appl. Phys.* **2012**, *112*, No. 014316.
(27) Chen, N.; Yang, R. T. Ab Initio Molecular Orbital Study of the Unified Mechanism and Pathways for Gas-Carbon Reactions. *J. Phys. Chem. A* **1998**, *102*, 6348.
(28) Chen, N.; Yang, R. T. Ab Initio Molecular Orbital Calculation on Graphite: Selection of Molecular System and Model Chemistry. *Carbon* **1998**, *36*, 1061.
(29) Backreedy, R.; Jones, J. M.; Pourkashanian, M.; Williams, A. A Study of the Reaction of Oxygen with Graphite: Model Chemistry. *Faraday Discuss.* **2001**, *119*, 385−394.
(30) Haynes, B. S. A Turnover Model for Carbon Reactivity I. Development. *Combust. Flame* **2001**, *126*, 1421−1432.
(31) Sendt, K.; Haynes, B. S. Density Functional Study of the Chemisorption of O_2 on the Armchair Surface of Graphite. *Proc. Combust. Inst.* **2005**, *30*, 2141−2149.
(32) Sendt, K.; Haynes, B. S. Density Functional Study of the Chemisorption of O_2 on the Zigzag Surface of Graphite. *Combust. Flame* **2005**, *143*, 629−643.
(33) Sendt, K.; Haynes, B. S. Modelling CO Desorption from Carbon Chars using Density Functional Theory, *5th Pacific Conference on Combustion*, 17−20 July, 2005.
(34) Radovic, L. R. Active Sites in Graphene and Mechanism of CO_2 Formation in Carbon Oxidation. *J. Am. Chem. Soc.* **2009**, *131*, 17166−17175.
(35) Radovic, L. R.; Silva-Tapia, A. B.; Vallejos-Burgos, F. Oxygen Migration on the Graphene Surface. 1. Origin of Epoxide Groups. *Carbon* **2011**, *49*, 4218−4225.
(36) Radovic, L. R.; Suarez, A.; Vallejos-Burgos, F.; Sofo, J. O. Oxygen Migration on the Graphene Surface. 2. Thermochemistry of Basal-Plane Diffusion (Hopping). *Carbon* **2011**, *49*, 4226−4238.
(37) Radovic, L. R.; Silva-Villalobos, A. F.; Silva-Tapia, A. B.; Vallejos-Burgos, F. On the Mechanism of Nascent Site Deactivation in Graphene. *Carbon* **2011**, *49*, 3471−3487.
(38) Silva-Tapia, A. B.; García-Carmona, X.; Radovic, L. R. Similarities and Differences in O_2 Chemisorption on Graphene Nanoribbon vs. Carbon Nanotube. *Carbon* **2012**, *50*, 1152−1162.
(39) Carlsson, J. M.; Scheffler, M. Structural, Electronic, and Chemical Properties of Nanoporous Carbon. *Phys. Rev. Lett.* **2006**, *96*, No. 046806.
(40) Carlsson, J. M.; Hanke, F.; Linic, S.; Scheffler, M. Two-Step Mechanism for Low-Temperature Oxidation of Vacancies in Graphene. *Phys. Rev. Lett.* **2009**, *102*, No. 166104.
(41) Allouche, A.; Ferro, Y. Dissociative Adsorption of Small Molecules at Vacancies on the Graphite (0001) Surface. *Carbon* **2006**, *44*, 3320−3327.
(42) Xu, S. C.; Chen, H.-L.; Lin, M. C. Quantum Chemical Prediction of Reaction Pathways and Rate Constants for Reactions of O_x (x = 1 and 2) with Pristine and Defective Graphite (0001) Surfaces. *J. Phys. Chem. C* **2012**, *116*, 1841−1849.
(43) Gürel, H. H.; Özçelik, C. O.; Ciraci, S. Dissociative Adsorption of Molecules on Graphene and Silicene. *J. Phys. Chem. C* **2014**, *118*, 27574−27582.
(44) Mehmood, F.; Pachter, R.; Lu, W.; Boeckl, J. J. Adsorption and Diffusion of Oxygen on Single-Layer Graphene with Topological Defects. *J. Phys. Chem. C* **2013**, *117*, 10366−10374.
(45) Qi, X.; Guo, X.; Zheng, C. Density Functional Study the Interaction of Oxygen Molecule with Defect Sites of Graphene. *Appl. Surf. Sci.* **2012**, *259*, 195−200.
(46) Guang, H.; Aoki, M.; Tanaka, S.; Kohyama, M. Hole Doping by Adsorption of Oxygen on a Stone = Thrower-Wales Defect in Graphene. *Solid State Commun.* **2013**, *174*, 10−15.
(47) Xu, S. C.; Irle, S.; Musaev, D. G.; Lin, M. C. Quantum Chemical Study of the Dissociative Adsorption of OH and H_2O on

DOI: 10.1021/acs.jpcc.8b10146
J. Phys. Chem. C 2018, 122, 29368−29379

Pristine and Defective Graphite (0001) Surfaces: Reaction Mechanisms and Kinetics. *J. Phys. Chem. C* **2007**, *111*, 1355−1365.
(48) Xu, S. C.; Irle, S.; Musaev, D. G.; Lin, M. C. Quantum Chemical Prediction of Pathways and Rate Constants for Reactions of CO and CO_2 with Vacancy Defects on Graphite (0001) Surfaces. *J. Phys. Chem. C* **2009**, *113*, 18772−18777.
(49) Xu, S. C.; Irle, S.; Lin, M. C. Quantum Chemical Prediction of Reaction Pathways and Rate Constants for Reactions of NO and NO_2 with Monovacancy Defects on Graphite (0001) Surfaces. *J. Phys. Chem. C* **2010**, *114*, 8375−8382.
(50) Nicholson, K. T.; Minton, T. K.; Sibener, S. J. Temperature-Dependent Morphological Evolution of HOPG Graphite upon Exposure to Hyperthermal O(^{3}P) atoms. *Prog. Org. Coat.* **2003**, *47*, 443−447.
(51) Nicholson, K. T.; Sibener, S. J.; Minton, T. K. Nucleation and Growth of Nanoscale to Microscale Cylindrical Pits in Highly-Ordered Pyrolytic Graphite upon Hyperthermal Atomic Oxygen Exposure. *High Perform. Polym.* **2004**, *16*, 197−206.
(52) Nicholson, K. T.; Minton, T. K.; Sibener, S. J. Spatially Anisotropic Etching of Graphite by Hyperthermal Atomic Oxygen. *J. Phys. Chem. B* **2005**, *109*, 8476−8480.
(53) Isborn, C. M.; Li, X.; Tully, J. C. Time-dependent Density Functional Theory Ehrenfest Dynamics: Collisions between Atomic Oxygen and Graphitic Clusters. *J. Chem. Phys.* **2007**, *126*, No. 134307.
(54) Paci, J. T.; Upadhyaya, H. P.; Zhang, L.; Minton, T.; et al. Theoretical and Experimental Studies of the Reactions Between Hyperthermal O(^{3}P) and Graphite: Graphene-Based Direct Dynamics and Beam-Surface Scattering Approaches. *J. Phys. Chem. A* **2009**, *113*, 4677.
(55) Sun, T.; Fabris, S.; Baroni, S. Surface Precursors and Reaction Mechanisms for the Thermal Reduction of Graphene Oxide. *J. Phys. Chem. C* **2011**, *115*, 4730−4737.
(56) Paci, J. T.; Minton, T. K.; Schatz, G. C. Hyperthermal Oxidation of Graphite and Diamond. *Acc. Chem. Res.* **2012**, *45*, 1973−1981.
(57) Morón, V.; Martin-Gondre, L.; Crespos, C.; Larregaray, P.; Gamallo, P.; Sayós, R. Classical Dynamics Study of Atomic Oxygen Over Graphite (0001) with New Interpolated and Analytical Potential Energy Surfaces. *Comput. Theor. Chem.* **2012**, *990*, 132−143.
(58) Poovathingal, S.; Schwartzentruber, T. E.; Srinivasan, S. G.; van Duin, A. C. T. Large Scale Computational Chemistry Modelling of the Oxidation of Highly Oriented Pyrolytic Graphite. *J. Phys. Chem. A* **2013**, *117*, 2692−2703.
(59) Murray, V. J.; Marshall, B. C.; Woodburn, P. J.; Minton, T. K. Inelastic and Reactive Scattering Dynamics of Hyperthermal O and O_2 on Hot Vitreous Carbon Surfaces. *J. Phys. Chem. C* **2015**, *119*, 14780−14796.
(60) Barinov, A.; Malcioglu, O. B.; Fabris, S.; Sun, T.; Gregoratti, L.; Dalmiglio, M.; Kiskinova, M. Initial Stages of Oxidation on Graphitic Surfaces: Photoemission Study and Density Functional Theory Calculations. *J. Phys. Chem. C* **2009**, *113*, 9009.
(61) Kane, J. J.; Karthik, C.; Ubic, R.; Windes, W. E.; Butt, D. P. An Oxygen Transfer Model for High Purity Graphite Oxidation. *Carbon* **2013**, *59*, 49−64.
(62) Kane, J. J.; Contescu, C. I.; Smith, R. E.; Strydom, G.; Windes, W. E. Understanding the Reaction of Nuclear Graphite with Molecular Oxygen: Kinetics, Transport, and Structural Evolution. *J. Nucl. Mater.* **2017**, *493*, 343−367.
(63) Mann, D. J.; Hase, W. L. Direct Dynamics Simulations of the Oxidation of a Single Wall Carbon Nanotube. *Phys. Chem. Chem. Phys.* **2001**, *3*, 4376−4383.
(64) Edel, R.; Grabnic, R.; Wiggins, B.; Sibener, S. J. Atomically-Resolved Oxidative Erosion and Ablation of Basal Plane HOPG Graphite Using Supersonic Beams of O_2 with Scanning Tunneling Microscopy Visualization. *J. Phys. Chem. C* **2018**, *122*, 14706−14713.
(65) Murray, V. J.; Smoll, E. J.; Minton, T. K. Dynamics of Graphite Oxidation at High Temperatures. *J. Phys. Chem. C* **2018**, *122*, 6602−6617.
(66) Jiang, D.; Sumpter, B. G.; Dai, S. First Principles Study of Magnetism in Nanographenes. *J. Chem. Phys.* **2007**, *127*, No. 124703.
(67) Hod, O.; Baorne, V.; Scuseria, G. E. Half-Metallic Graphene Nanodots: A Comprehensive First-Principles Theoretical Study. *Phys. Rev. B* **2008**, *77*, No. 035411.
(68) Jiang, D.; Dai, S. Circumacenes Versus Periacenes: HOMO-LUMO Gap and Transition from Nonmagnetic to Magnetic Ground State with Size. *Chem. Phys. Lett.* **2008**, *466*, 72−75.
(69) Moscardó, F.; San-Fabian, E. On the Existence of Spin-Polarized State in the n-Periacene Molecules. *Chem. Phys. Lett.* **2009**, *480*, 26−30.
(70) Plasser, F.; Pašalić, H.; Gerzabek, M. H.; Libisch, F.; Reiter, R.; Burgdörfer, J.; Müller, T.; Shepard, R.; Lischka, H. The Multiradical Character of One- and Two-dimensional Graphene Nanoribbons. *Angew. Chem., Int. Ed.* **2013**, *52*, 2581−2584.
(71) Horn, S.; Plasser, F.; Müller, T.; Libisch, F.; Burgdörfer, J.; Lischka, H. A Comparison of Singlet and Triplet States for One- and Two-dimensional Graphene Nanoribbons Using Multireference Theory. *Theor. Chem. Acc.* **2014**, *133*, 1511.
(72) Torres, A. E.; Guadarrama, P.; Fomine, S. Multiconfigurational Character of the Ground States of Polycyclic Aromatic Hydrocarbons. A Systematic Study. *J. Mol. Model.* **2014**, *20*, No. 2208.
(73) Pykal, M.; Jurečka, P.; Karlicky, F.; Otyepka, M. Modelling of Graphene Functionalization. *Phys. Chem. Chem. Phys.* **2016**, *18*, 6351.
(74) Stewart, J. J. P. Optimization of Parameters for Semiempirical Methods VI: More Modifications to the NDDO Approximations and Re-optimization of Parameters. *J. Mol. Model.* **2013**, *19*, 1−32.
(75) Stewart, J. P. MOPAC2012; *Stewart Computational Chemistry*: Colorado Springs: CO, http://OpenMOPAC.net, 2012.
(76) Frankcombe, T. J. Spin State Splitting in Carbon Gasification Models. *J. Phys. Chem. A* **2009**, *113*, 3299−3302.
(77) Pham, B. Q.; Truong, T. N. Electronic Spin Transitions in Finite-Size Graphene. *Chem. Phys. Lett.* **2012**, *535*, 75−79.
(78) Moscardó, F.; San-Fabián, E. On the Existence of a Spin-Polarized State in the n-Periacene Molecules. *Chem. Phys. Lett.* **2009**, *480*, 26−30.
(79) Banerjee, S.; Bhattacharyya, D. Electronic Properties of Nanographene Sheets Calculated Using Quantum Chemical DFT. *Comput. Mater. Sci.* **2008**, *44*, 41−45.
(80) Liu, L.; Chen, S. Geometries and Electronic States of Divacancy Defect in Finite-Size Hexagonal Graphene Flakes. *J. Chem.* **2017**, *2017*, No. 8491264.
(81) Tachikawa, H.; Nagoya, Y.; Kawabata, H. A Density Functional Theory Study of Ground and Low-lying Excited Electronic States in Defective Graphenes. *J. Chem. Theory Comput.* **2009**, *5*, 2101−2107.
(82) Hu, X.; Hase, W. L.; Pirraglia, T. Vectorization of the General Monte Carlo Classical Trajectory Program VENUS. *J. Comput. Chem.* **1991**, *12*, 1014−1024.
(83) Hase, W. L.; Duchovic, R. J.; Hu, X.; Komornicki, A.; Lim, K. F.; Lu, D. H.; Peslherbe, G. H.; Swamy, K. N.; Vande Linde, S. R.; Zhu, L.; et al. VENUS. A General Chemical Dynamics Computer Program. *QCPE Bull.* **1996**, *16*, 671.
(84) Song, K.; de Sainte Claire, P.; Hase, W. L.; Hass, K. C. Comparison of Molecular Dynamics and Variational Transition-State-Theory Calculations of the Rate Constant for 8-Atom Association with the Diamond [111] Surface. *Phys. Rev. B.* **1995**, *52*, 2949−2957.
(85) Schlier, C.; Seiter, A. Symplectic Integration of Classical Trajectories: A Case Study. *J. Phys. Chem. A* **1998**, *102*, 9399−9404.
(86) Schlier, C.; Seiter, A. High-order Symplectic Integration: An Assessment. *Comput. Phys. Commun.* **2000**, *130*, 176−189.
(87) Tachikawa, H.; Kawabata, H. Electronic states of Defect Sites of Graphene Model Compounds: A DFT and Direct Molecular Orbital-Molecular Dynamics Study. *J. Phys. Chem. C* **2009**, *113*, 7603−7609.
(88) Murray, V. J.; Marshall, B. C.; Woodburn, P. J.; Minton, T. K. Inelastic and Reactive Scattering Dynamics of Hyperthermal O and O_2 on Hot Vitreous Carbon Surfaces. *J. Phys. Chem. C* **2015**, *119*, 14780−14796.

DOI: 10.1021/acs.jpcc.8b10146
J. Phys. Chem. C 2018, 122, 29368−29379

(89) Olander, D. R.; Schwarz, J. A.; Siekhaus, W.; Jones, R. Reactions of Modulated Molecular-Beams with Pyrolytic-Graphite: 1. Oxidation of Basal Plane. *J. Chem. Phys.* **1972**, *57*, 408−420.
(90) Wiggins, B.; Avila-Bront, L. G.; Edel, R.; Sibener, S. J. Temporally and Spatially Resolved Oxidation of Si (111)-(7 × 7) Using Kinetic Energy Controlled Supersonic Beams in Combination with Scanning Tunneling Microscopy. *J. Phys. Chem. C* **2016**, *120*, 8191−8197.
(91) Ranish, J. M.; Walker, P. L., Jr. High-Pressure Studies of the Carbon-Oxygen Reaction. *Carbon* **1993**, *31*, 135−141.
(92) Malola, S.; Hakkinen, H.; Koskinen, P. Comparison of Raman Spectra and Vibrational Density of States Between Graphene Nanoribbons with Different Edges. *Eur. Phys. J. D* **2009**, *52*, 71−74.
(93) Goodman, F. O.; Wachman, H. Y. *Dynamics of Gas-Surface Scattering*; Academic Press: New York, 1976.
(94) Lehtinen, O.; Kotakoski, J.; Krasheninnikov, A. V.; Tolvanen, A.; Nordlund, K.; Keinonen, J. Effects of Ion Bombardment on a Two-dimensional Target: Atomistic Simulations of Graphene Irradiation. *Phys. Rev. B* **2010**, *81*, No. 153401.
(95) Yoon, K.; Rahnamoun, A.; Swett, J. L.; Iberi, V.; Cullen, D. A.; Vlassiouk, I. V.; Belianinov, A.; Jesse, S.; Sang, X.; Ovchinnikova, O.S.; et al. Atomistic-Scale Simulations of Defect Formation in Graphene under Noble Gas Ion Irradiation. *ACS Nano* **2016**, *10*, 8376−8384.
(96) Skowron, S. T.; Lebedeva, I. V.; Popovc, A. M.; Bichoutskaia, E. Energetics of Atomic Scale Structure Changes in Graphene. *Chem. Soc. Rev.* **2015**, *44*, 3143.

DOI: 10.1021/acs.jpcc.8b10146
J. Phys. Chem. C 2018, 122, 29368−29379